Paper

1 First Part

2 Data and Sample Selection

- We select JWST AGNs by compiling the literature on spectroscopic observation of AGNs with NIRSpec or NIRCam grism identified in the following public fields: the JWST Advanced Deep Extragalactic Survey. First Reionization Epoch Spectroscopically Complete Observations (FRESCO); Cosmic Evolution Early Release Science Survey (CEERS); Public Release IMaging for Extragalactic Research (PRIMER) survey.

- We note that some of the JWST AGNs in the **CEERS**[*Cosmic Evolution Early Release Science Survey*] field are excluded because they are located in the region where only **NIRSpec** observation is performed, hence there are no catalogued galaxies with **NIRCam** photometry around them.

  - This paragraph explains that certain JWST-detected AGNs in the CEERS field were excluded from the analysis because they were located in areas where only NIRSpec observations (spectroscopic data) were conducted, without corresponding NIRCam observations (imaging data).

    NIRCam photometry is essential for cataloging nearby galaxies in the field, providing information on the photometric properties and spatial distribution of galaxies around these AGNs. Without this NIRCam data, researchers lack the necessary photometric information to analyze the clustering of galaxies around those AGNs. Consequently, any AGNs located in regions with only NIRSpec data were removed from the sample to ensure that all selected AGNs are in areas where both NIRSpec and NIRCam data are available. This allows for a consistent clustering analysis.

  - We only use spectroscopically confirmed AGNs with broad Balmer line components with FWHM $\gtrsim$ 1000 km s -1 , i.e., the same feature as type-1 AGNs. AGNs with only narrow Balmer lines that do not meet the above conditions are excluded here, because the clustering strength of obscured AGNs may differ from that of type-1 AGNs.

- We only use spectroscopically confirmed AGNs with broad Balmer line components with FWHM $\gtrsim$ 1000 km s -1 , i.e., the same feature as type-1 AGNs. AGNs with only narrow Balmer lines that do not meet the above conditions are excluded here, because the clustering strength of obscured AGNs may differ from that of type-1 AGNs.

  - **Broad Balmer Lines**: The Balmer lines are specific spectral lines produced by hydrogen. In type-1 AGNs, these lines are *broad* due to the rapid motion of gas near the supermassive black hole. A broad line width (here, FWHM $\geq$ 1,000 km/s) indicates that the gas is moving at high velocities, typical of type-1 AGNs where the central black hole and its surrounding gas are directly visible.

  - **Excluding Narrow-Line AGNs**: The study excludes AGNs that show only narrow Balmer lines (lower velocity gas), as narrow lines are typically found in obscured, or type-2, AGNs. This exclusion is important because the clustering properties of obscured (type-2) AGNs may differ from those of unobscured (type-1) AGNs, potentially complicating the analysis.

- No limits are placed on the luminosity of JWST AGNs, assuming that the clustering strength of the JWST AGN, like the type-1 AGN, is independent of luminosity and we emphasise that this analysis does not need the intrinsic bolometric luminosity, which may be underestimated due to heavy obscuration of JWST AGNs.

    - This paragraph explains that the researchers did not set a minimum or maximum luminosity requirement for the JWST AGNs included in their study. They made this decision based on the assumption that the clustering strength (the tendency of AGNs to be spatially grouped) does not depend on the luminosity of the AGNs, meaning that brighter or fainter AGNs should cluster similarly.

    - They assume that the clustering properties of AGNs are the same regardless of luminosity, allowing them to include a range of AGNs in their analysis without concern that clustering strength will vary across different brightness levels.

    - They also point out that their analysis does not require knowing the AGNs' *intrinsic bolometric luminosity* (the total energy emitted across all wavelengths). This is because, *in some AGNs, heavy obscuration (dense material blocking light from the AGN) can make the observed luminosity appear lower than it actually is.* By not relying on luminosity, they avoid potential inaccuracies from obscured AGNs appearing fainter than their true output.

- Although no limits are set for luminosity, in the end, the AGNs selected by JWST are limited to those with lower luminosity ($-17 < \boldsymbol{MUV} < -20$) than quasars.

- Figure 1 shows the redshift distribution of JWST AGNs in the literature, showing that the number is the highest at $5 < z < 6$. Hence, we select JWST AGNs at $5 < z < 6$ (hatched region in Figure 1) for the clustering analysis.

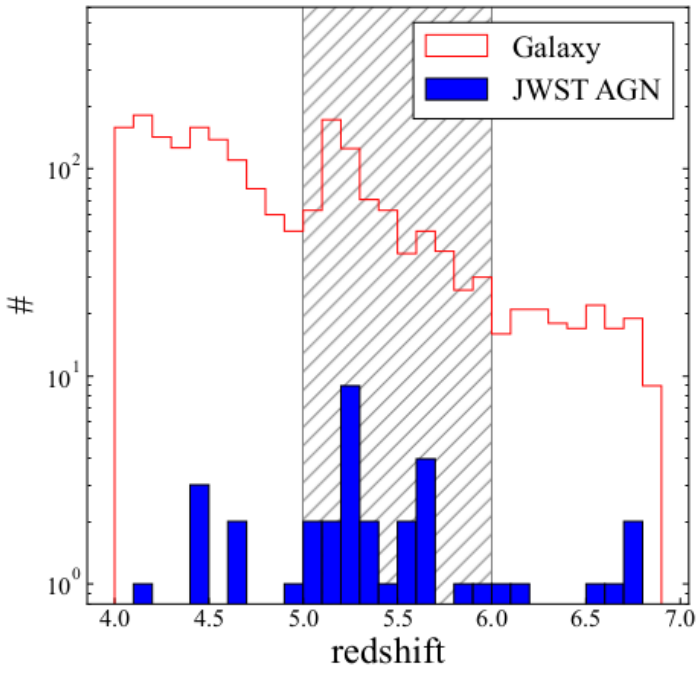

Figure 1. The redshift distribution based on spectroscopic redshifts of JWST AGNs (blue) and photometric redshirts of galaxies (red) samples in the compilation of the literature (Maiolino et al. 2023; Harikane et al. 2023; Kocevski et al. 2024; Matthee et al. 2024). The hatched region shows the galaxy and AGN samples utilised in this analysis.

- We try detecting the clustering signal of JWST AGNs at $z < 5$ or $z > 6$, but the signal is hardly detected due to their low surface number density at the redshift ranges. The final sample contains 28 JWST AGNs at $5 < z < 6$.

- We make use of the galaxy catalogue from DAWN JWST Archive (DJA). DJA catalogues are created based on the public data of JWST surveys, which are reduced with grizli2 (Brammer 2023a) and msaexp3 (Brammer 2023b) by the Cosmic Dawn Center.

  - **Source of the Catalog**: The DAWN JWST Archive (DJA) catalog compiles data from public JWST surveys. It is produced by the Cosmic Dawn Center and combines observations from both the JWST and the Hubble Space Telescope (HST).

  - The data in DJA is processed with two tools: **grizli** (developed by Brammer in 2023) and **msaexp**. These tools help calibrate and prepare the JWST data for analysis, ensuring accurate and consistent measurements.

- The catalogues contain photometric redshifts of galaxies estimated by EAZY4 (Brammer et al. 2008) with JWST and Hubble Space Telescope (HST) photometry.

  - **Photometric Redshifts**: The DJA catalog provides *photometric redshifts* for galaxies, which estimate the galaxy distances by analyzing their light across multiple wavelengths. These estimates were calculated using **EAZY**, a software tool that models galaxy colors based on known galaxy templates.

- We use the v7 catalogues of three survey fields: Great Observatories Origins Deep Survey North and South; CEERS; PRIMER. We note that the GOODS-North and GOODS-South catalogues contain JADES and FRESCO data.

  - **Survey Fields Used**: The researchers use version 7 (v7) of the DJA catalog, specifically focusing on data from three key JWST survey fields:

  - **GOODS-North** and **GOODS-South**: Part of the Great Observatories Origins Deep Survey, aimed at studying galaxies over a range of redshifts.

  - **CEERS**: The Cosmic Evolution Early Release Science Survey, targeting galaxy formation and evolution.

  - **PRIMER**: Another JWST survey contributing to galaxy observations.

- We select the bright galaxies from the catalogues by the following criteria:

  $5 < z\mathrm{phot} < 6$; & $n\mathrm{filter} \geq 12$; & $23 < \mathrm{F444W} < 26$,

  where z phot is the photometric redshift by EAZY and $n$filter represents the number of filters utilised to estimate the photometric redshift.

- We use an aperture magnitude with a diameter of $0.''5$. We exclude faint galaxies with $\mathrm{F444W} > 26$ from the catalogue so that the depth of the limiting magnitude is uniform over the survey field.

  - **Excluding Faint Galaxies (F444W $>$ 26)**: Galaxies with an F444W (near-infrared filter) magnitude greater than 26 are excluded because they are too faint. By setting this limit, the researchers ensure that all galaxies in the sample are *bright enough to be uniformly detectable* across the entire survey area, avoiding inconsistencies in sensitivity.

- As Figure 2 in Merlin et al. (2024), most of the fields show better sensitivity than 27 mag, which supports that the bright galaxies with $\mathrm{F444W} < 26$ are homogeneously detectable.

- We exclude extremely bright objects with $\mathrm{F444W} < 23$ because some of them may be no extragalactic objects.

- Homogeneous selection of galaxies promises reliable cross-correlation analysis to derive the typical DMH mass of JWST AGNs, although JWST AGNs are not selected homogeneously.
  - By selecting galaxies within a defined brightness range ($23 < \mathrm{F444W} < 26$), the sample is more homogeneous. This consistency is crucial for accurately measuring the spatial clustering and estimating the dark matter halo (DMH) masses of JWST AGNs. Even though the JWST AGNs themselves aren't selected as homogeneously, a uniform galaxy sample allows for reliable cross-correlation analysis.
- Although we do not exclude galaxies with poor EAZY template fitting, we confirm that the clustering strength does not change even when we limit the sample with the goodness of fit, $\chi^2_\nu < 5$. Finally, our sample contains 679 galaxies that are distributed over 409.3 arcmin2 , and their breakdowns are summarised in Table 1.
  - Although they don't exclude galaxies based on poor template fitting in EAZY (a software tool for photometric redshift estimation), they tested whether limiting the sample to well-fitted galaxies would affect clustering strength. It did not, even with a tighter fit criterion $\chi^2_\nu < 5$.
  - **Final Sample**: The final galaxy sample includes 679 galaxies distributed over an area of 409.3 arcminutes squared. These galaxies are summarized in Table 1 of the study.

Field	Effective area (arcmin^2)	N_{galaxy} (#)	N_{AGN} (#)	Reference
GOODS North	85.7	200	12	Maiolino et al. (2023); Matthee et al. (2024)
GOODS South	62.1	69	2	Maiolino et al. (2023); Matthee et al. (2024)
CEERS	95.3	207	12	Harikane et al. (2023); Kocevski et al. (2024)
PRIMER-UDS	166.2	203	2	Kocevski et al. (2024)
Total	409.3	679	28	

3 Clustering Analisis

We first evaluate the angular cross-correlation function $\omega(\theta)$ in Section 3.1 taking into account that photometric redshift, whose uncertainty is larger than that of spectroscopic redshift, is only available for the galaxy sample. However, we note that the uncertainty of the photometric redshift is much smaller than the redshift range of the galaxy sample. We also evaluate the projected correlation function $\omega\ p\ (r\ p\ )$ of each subsample in Section 3.2 to check the robustness of the result.

We note that these measurements of the typical DMH mass are independent. We adopt almost the same way to evaluate the correlation functions in Arita et al. (2023); therefore we briefly describe the method.

3.1 Angular correlation function

We evaluate the angular cross-correlation function between JWST AGNs and galaxies, ωCCF (θ), and the angular auto-correlation function of galaxies, ωACF (θ). We use the following estimators to evaluate the correlation functions:

$$\omega_{CCF}(\theta) = \frac{D_{AGN}D_{\mathrm{galaxy}} - D_{AGN}R - D_{\mathrm{galaxy}}R + RR}{RR}$$

$$\omega_{CCF}(\theta) = \frac{D_{\mathrm{galaxy}}D_{\mathrm{galaxy}} - 2D_{\mathrm{galaxy}}\,R - D_{\mathrm{galaxy}}R + RR}{RR}$$

Where:

- $D_{AGN}D_{\mathrm{galaxy}}$: normalised number of pairs between AGNs and galaxies.
- $D_{AGN}R$: AGNs and random points.

- $D_{\rm galaxy}\,R$: galaxies and random points
- RR : random points and random points
- $D_{\rm galaxy}D_{\rm galaxy}$: galaxies and galaxies

within the specified angular range, respectively.

The random points are scattered over the survey region at a surface number density of $100\,\mathrm{arcmin}^{-2}$. In order to trace the survey fields, we only use the random points located within $3''$ of objects with $n_{\rm filter} \geq 12$. We evaluate both cross- and auto-correlation functions at $\theta > 10''$ to avoid the one-halo term.

- This paragraph describes how the researchers created and used a set of random points to perform correlation analyses of galaxies and AGNs in the survey.
- By carefully generating and filtering random points, and by excluding small-scale clustering, the researchers ensure that their cross- and auto-correlation analyses are robust and reflect large-scale structure rather than local effects. This helps in deriving properties like the typical dark matter halo mass associated with JWST AGNs and their surrounding galaxies.
- To accurately reflect the structure of the survey fields (regions observed by JWST), the random points are limited to areas near real observed objects. Specifically, random points are only kept if they are within **3 arcseconds** of galaxies that were observed with at least **12 filters** ($n_{\rm filter} \geq 12$).
- This restriction ensures that the random points match the spatial distribution and coverage of the actual data, avoiding biases introduced by unobserved regions.
- **Cross-Correlation Function**: Measures the clustering between two different types of objects (e.g., JWST AGNs and galaxies).
- **Auto-Correlation Function**: Measures the clustering of a single type of object (e.g., galaxies with themselves).
- Correlations at small angular scales $\theta < 10''$ are dominated by the **one-halo term**, which reflects clustering within the same dark matter halo (e.g., galaxies close to each other within a single halo). This term is excluded because the focus is on larger-scale clustering between distinct halos, represented by the **two-halo term**. To avoid this small-scale effect, only separations greater than 10 arcseconds are included in the analysis.

The uncertainties are estimated by the bootstrap resampling with $N = 1000$ times iteration. We randomly select the same number of JWST AGNs and galaxies from the sample allowing duplication and evaluate the cross- and auto-correlation functions for each subsample. We calculate the covariance matrix below and the diagonal element shows the uncertainty of each bin:

$$C_{i,j} = \frac{1}{N-1}\sum_{k=1}^{N} (\omega_i^k - \bar{\omega}_i)(\omega_j^k - \bar{\omega}_j)$$

Where: ω_i^k: correlation function in ith bin of kth iteration. $\bar{\omega_i}$: mean value of the correlation function in ith bin.

- This paragraph explains how the researchers estimate uncertainties in their clustering analysis using **bootstrap resampling**. This statistical technique provides a way to assess the reliability of their results by repeatedly sampling from the data.
- **Bootstrap Resampling**:
    - The researchers perform $N = 1000$N=1000 bootstrap iterations. In each iteration, they randomly select the same number of AGNs and galaxies from the original sample, allowing some objects to be selected multiple times (duplication) while others may be excluded.

- This creates 1000 different subsamples, each slightly varying from the original, which helps evaluate the variability in the clustering measurements.

– For each bootstrap subsample, they recalculate the **cross-correlation function** (clustering between AGNs and galaxies) and the **auto-correlation function** (clustering of galaxies with themselves).

– This repeated calculation provides a distribution of clustering values for each angular bin, reflecting how results might fluctuate due to random sampling effects.

– The **covariance matrix** is a statistical tool that quantifies the uncertainty and correlation between different bins of the correlation function. It's calculated from the clustering results of all bootstrap iterations.

– The **diagonal elements** of the covariance matrix represent the **variance** (or squared uncertainty) for each bin. Taking the square root of these diagonal elements gives the uncertainty for the clustering measurement in each bin.

Figure 2 shows ω_{CCF} (red) and ω_{ACF} (blue). The red and blue solid lines show the best fit of a power-law function. Regarding the integral constraint due to the limited survey area (Groth & Peebles 1977), we confirm that it can be negligible in a scale of $\theta \lesssim 100''$. Hence, we ignore the integral constraint in this analysis.

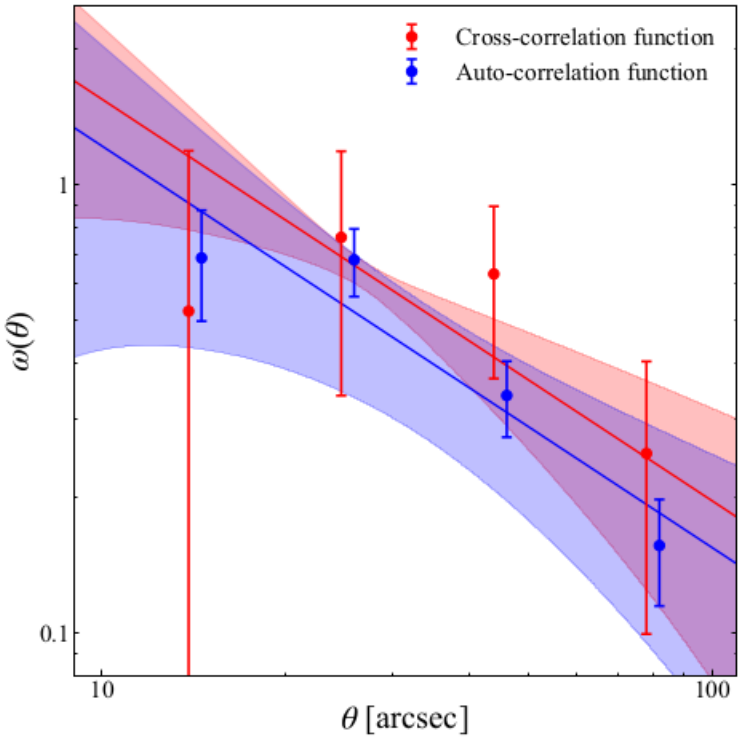

Figure 2. Angular correlation functions and the results of the MCMC fit (blue: auto-correlation function; red: cross-correlation function). The solid lines represent the best estimates of the power-law function $\omega(\theta) = (\theta/\theta_0)^{-\beta}$ fitted to the correlation functions. The shaded region denotes the power-law functions with parameters in each MCMC step.

We use a Markov Chain Monte Carlo (MCMC) algorithm (Foreman-Mackey et al. 2013) to fit the simple powerlaw function, $\omega(\theta) = (\theta/\theta\ 0\ ) -\beta$ .We assume a Gaussian likelihood function and uniform priors for $\theta\ 0 \in [1'', 100'']$ and the slope $\beta \in [0, 2]$. We define the best estimate as the median and 16th and 84th percentiles of the posterior distribution. First, we perform MCMC fit for

the auto-correlation function because the signal-to-noise ratio is better than the cross-correlation function. We obtain θ 0,ACF = 11.″ 90+2.30 −2.79 and β = 0.90+0.16 as the best estimate. The cross-correlation −0.16 function uses the same β obtained in the MCMC fit to the auto-correlation function and evaluates θ 0 for the fixed-β in each MCMC step. Finally, we obtain θ_0 for the cross-correlation function as θ 0,CCF = 16.″ 33+0.99

- The clustering signal is modeled with a simple power-law function:

$$\omega(\theta) = \left(\frac{\theta}{\theta_0}\right)^{-\beta}$$

  θ_0: The *characteristic angular scale*, representing the strength of clustering.

  β: The *slope* of the power law, describing how clustering decreases with angular separation.

- They use an **MCMC algorithm** (from Foreman-Mackey et al., 2013) to explore the parameter space of θ_0 and β find the best-fit values.

- **MCMC**: A computational technique that estimates the probability distribution of parameters by generating samples from the parameter space, based on the observed data and a likelihood function.

- **Likelihood Function**: Assumed to be Gaussian, meaning the observed data are fit as if they follow a normal distribution around the model.

- **Uniform Priors**: The parameter ranges are assumed to have equal probability within these intervals:

  $\theta_0 \in [1'', 100'']$, $\beta \in [0, 2]$

- The best-fit parameters are defined using the **median** of the posterior distributions from the MCMC samples, with uncertainties given by the **16th and 84th percentiles** (analogous to $\pm 1\sigma$ in a Gaussian distribution).

- They first fit the **auto-correlation function (ACF)** because it has a higher signal-to-noise ratio than the cross-correlation function (CCF), providing more reliable parameter estimates.

- The best-fit values for the ACF are:

  $\theta_{0,\mathrm{ACF}} = 11.90'' \,^{+2.30}_{-2.79}$, $\beta = 0.90^{+0.16}_{-0.16}$(slope)

- For the **cross-correlation function (CCF)**, they fix the slope $\beta\beta$ to the value obtained from the ACF fit $\beta = 0.90$

- Then, they evaluate θ_0 for the CCF by running MCMC with this fixed β.

Saltar al paso 4 porque es muy tecnico todo.

4 Discussion

4.1 Comparison of typical DMH mass of JWST AGNs and quasars

We **compare** the typical ***DMH mass*** of JWST AGNs with that of ***quasars*** derived by the clustering analysis. Figure 4 **summarises** the DMH mass measurement of quasars at $0 \lesssim z \lesssim 6.5$ (Shen et al. 2007; Ross et al. 2009; Eftekharzadeh et al. 2015; He et al. 2018; Timlin et al. 2018; Arita et al. 2023; Eilers et al. 2024).

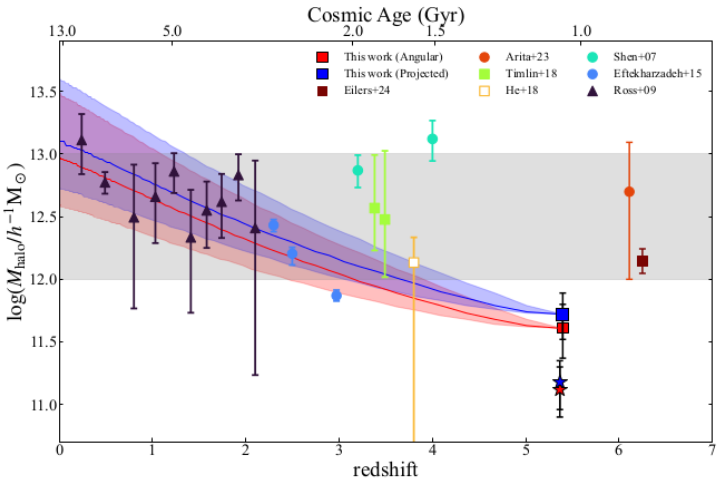

Figure 4. Comparison of DMH mass of JWST AGNs in this study (blue square: angular, red square: projected) with those in literature based on the clustering analysis. We also show the DMH mass of galaxies as stars. The symbols of previous studies are classified by type of correlation function (circle: projected correlation function, square: angular correlation function, triangle: redshift-space correlation function). The filled and open symbols show the auto-correlation function and the cross-correlation function is used to estimate the typical DMH mass. We note that the DMH masses in the previous studies have been converted to those using cosmological parameters in this study and their bias parameters, because some cosmological parameters, particularly σ_8, have a large impact on the DMH mass estimate. The grey-shaded region shows the typical DMH mass range of quasars suggested by Trainor & Steidel (2012); Shen et al. (2013); Timlin et al. (2018); Arita et al. (2023). The solid lines with the shaded regions denote the mass evolution of DMH hosting JWST AGNs at $5 < z < 6$ and its 1σ error calculated by the extended Press-Schechter theory.

The previous clustering analysis indicates that type-1 quasars have a nearly constant halo mass of $\log(M\text{halo}\ /h\ -1\ \text{M}\ \odot\ ) \sim 12.5$ through the cosmic time (Trainor & Steidel 2012; Shen et al. 2013; Timlin et al. 2018; Arita et al. 2023).

Arita et al. (2023) discuss the possibility that there is a ubiquitous mechanism that activates quasars only in the DMHs with $12 \lesssim \log(M\text{halo}\ /h\ -1\ \text{M}\ \odot\ ) \lesssim 13$ (grey region in Figure 4).

In contrast, the typical DMH mass of JWST AGNs is lower than theirs by ~ 1 dex, **implying** that **JWST AGNs may be different populations than type-1 quasars**.

Pizzati et al. (2024b) **predicts** that the **DMH mass** of LRDs **should be smaller** than that of **unobscured quasars** from their large abundance difference.

- In this context, **LRD** stands for **Lightly Reddened Object**. These are active galactic nuclei (AGNs) that are partially obscured by dust but not as heavily obscured as Type-2 AGNs.

Although our sample is **not necessarily identica**l to the LRDs, the DMH mass by the clustering analysis is **consistent** with the **theoretical prediction**.

No examples of DMH masses as less massive as the JWST AGNs in this study have been measured even in the faint type-1 quasars at low-z.

- Ne se han encontrado masas de DMH tan poco masivas como las de los AGN de JWST en el estudio

The DMH mass of JWST AGN is rather consistent with that of the galaxy sample within 1σ errors.

Given that they are **different populations**, *there is no need for the abundance of the JWST AGNs* on the luminosity function *to coincide with the type-1 quasar's extension to the faint-end*, nor is there a need for the JWST AGN to follow the MBH -$M*$ relation formed by the type-1 AGNs.

- **JWST AGNs are distinct from type-1 quasars** based on their clustering properties, luminosities, and dark matter halo (DMH) masses.
- As a result, **their abundance on the luminosity function does not need to align with type-1 quasars**:
  - JWST AGNs don't have to extend the type-1 quasar luminosity function to fainter luminosities because they may not evolve or form in the same way.

– No Obligation to Follow the $M_{BH} - M_*$ - Relation: The $M_{BH} - M_*$ relation describes the correlation between the mass of the central black hole (M_{BH}) and the stellar mass of the host galaxy (M_*).

– For type-1 AGNs, this relation reflects co-evolution between the black hole and the host galaxy over cosmic time.

– JWST AGNs are not required to follow this relation: Since they may evolve differently, their black hole growth and host galaxy properties could diverge from the trends observed in type-1 quasars.

– KEY: The **abundance** and **physical properties** of JWST AGNs suggest they are not merely lower-luminosity counterparts of type-1 quasars but a distinct class of AGNs.

However, since the lower limit of the mass range of typical quasars has not been rigorously measured, it is possible that faint quasars with $\boldsymbol{M}1450 \gtrsim -20$ reside in less massive DMHs with $\log(\boldsymbol{M}\mathrm{halo}\ /h\ -1\ \mathrm{M}\odot) < 12$.

Hence, the possibility that the JWST AGNs that are typically faint ($\boldsymbol{M}1450 \gtrsim -20$) are new type-1 quasars hosted by less massive DMHs not previously found cannot be ruled out. (Explanation)

On the other hand, Allevato et al. (2014) reported that DMH mass of X-ray-selected type-2 AGNs at $z \sim 3$ is estimated as $\log(\boldsymbol{M}\mathrm{halo}\ /h\ -1\ \mathrm{M}\odot) = 11.73{+}0.39\ -0.45$, which is consistent with our measurements.

However, there are contradicting measurements of DMH mass for type-2 AGNs. Allevato et al. (2011) showed that X-ray-selected narrow-line AGNs at $0.6 \leq z \leq 1.5$ are hosted by massive DMHs with $\log(\boldsymbol{M}\mathrm{halo}\ /h\ -1\ \mathrm{M}\odot) \sim 13.00 \pm 0.06$.

Viitanen et al. (2023) indicated that the DMH mass of X-ray-selected AGNs does not depend on their obsculation and that the typical DMH mass is $\log(\boldsymbol{M}\mathrm{halo}\ /h\ -1\ \mathrm{M}\odot) = 12.98{+}0.17$ $(12.28{+}0.13)$ at $z \sim 0.7(1.8)$.

The $-0.22\ -0.19$ DMH mass of JWST AGNs is less massive than that of X-ray selected AGNs (Krishnan et al. 2020) at $0 < z < 2.5$, hosted on average in DMHs of 1012-13 $h\ -1\ \mathrm{M}\odot$.

We calculate the redshift evolution of the DMH mass of JWST AGNs based on the Extended Press-Schechter theory (e.g. Bower 1991). The red and blue solid lines in Figure 4 show the evolution of the DMH mass with $\log(\boldsymbol{M}\mathrm{halo}\ /h\ -1\ \mathrm{M}\odot) = 11.61, 11.72$ at $z = 5.4$, respectively.

We find that the DMHs hosting JWST AGNs grow to as massive as $\sim 1013\ h\ -1\ \mathrm{M}\odot$ at $z = 0$, which is comparable to the DMH mass of a galaxy cluster in the local Universe.

Furthermore, we find that the DMH mass of JWST AGNs will reach 1012-13 $h\ -1\ \mathrm{M}\odot$, a typical type-1 quasar's DMH mass regime, at $z \lesssim 3$.

This recalls a scenario where the JWST AGNs at $5 < z < 6$ will grow into quasars at $z \lesssim 3$. In other words, the **JWST AGNs at $5 < \boldsymbol{z} < 6$ are the ancestors of quasars at $\boldsymbol{z} \lesssim 3$** and will start to shine as quasars in ~ 1 Gyr later.

Here, from the perspective of DMH mass evolution, it can be reasonably explained that the DMH hosting the JWST AGN will grow to be comparable to the DMH at $z < 3$ quasar, but please **note that this does not guarantee that the JWST AGN will necessarily grow to be a quasar**.

According to Hopkins et al. (2008), an evolution model of quasars induced by a major merger, $\sim$ 1 Gyr before a quasar phase corresponds to a coalescence phase. The model predicts that after the coalescence phase, a starburst occurs, significantly increasing the stellar mass of the host galaxy, and if this is correct, then at $z \sim 3$, the overmassive situation in JWST AGNs (Maiolino et al. 2023; Harikane et al. 2023) is supposed to be mitigated.

The possibility of the episodic intense starburst for JWST AGNs is remarked in Kokorev et al. (2024a) based on their JWST observation for a LRD at $z = 4.13$, which is consistent with the scenario. The details on the relation between the host stellar mass and the SMBH mass are discussed in Section 4.2.

5 Resumen

For AGNs of low luminosity provided by JWST, they want to know de DMH mass, and to do that, they will perform clustering analysis.

The sample they work with is: 28 AGN and 679 Galaxies. The AGNs are in the range of $5 < z < 6$.

What they find is:

1) The angular cross-correlation and the Projected cross-correlation say:

angular cross-correlation : Halo Mass = 11.61

Projected cross-correlation : Halo Mass = 11.72

This mases are 1 exponente less that the masses found by Tipical DMH of quasars in $0 < z < 6$ derived by clustering analysis.

2) The press schechter theory predicts that this AGNs will evolve so that their mases will grow up to exponent 12 to 13 and that is the thypical mass of quasars at $z < 3$. And this may imply that this AGNs are ancestors of this quasars.

3) About the galaxies that hosts these AGNs, they found that their stellar masses are: 9.72 to 9.90. This is being measured based on DMH mass and the empirical stellar-to-halo mass ratio.

he mass is consistent with the inferred stellar mass in Akins et al. (2024). And describes the methodology they used.

4) If we assume that JWST AGNs are the ancestor of $z < 3$ quasars then they speculated about JWST AGNs will experience a starburst at later stage. This speculation is based on the model of Hopkins et al. (2008). When they experience the starbust they will approach the local MBH -$M*$ relation.

They elaborated on this possibility and they found that they approach to the local relation given by Sun et al. (2024).

For the following conclusion we need this definition: The **duty cycle** of AGNs, $f_{\rm duty}$, is defined as the time fraction of their active phase in the cosmic age.

In another way, it is the time that the AGN is active.

5) They calculate this duty cycle. To calculate this, they asume that a DMH of mass ,exponent, of 11 to 12 can Host the AGN and that *AGN can shine in a certain period randomly.*

And what they have obtained is the following duty cycle: $f_{\rm duty} = 0.36$ percent. This duty cicle is comparable to quasars at $z < 4$ and is 1-2 dex higher than quasars at $z = 6$.

6) Based on the DMH mass obtained plus some other observational properties, they postulate that this AGNs could be:

a) Precursors of quasars at $z < 3$

b) A different AGN population

c) Maybe this AGNs are just *low-mass type 1 quasars*.

d) They are not AGN objects.